Engineering Structures 309 (2024) 118058

Contents lists available at ScienceDirect

Engineering Structures

journal homepage: www.elsevier.com/locate/engstruct

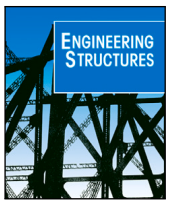

# Anisotropy and compaction gradient assessment on rammed earth specimens through sonic tomography approach

J.D. Rodríguez-Mariscal [a], M. Zielińska [b], M. Rucka [c], M. Solís [a,*]

[a] Department of Continuum Mechanics and Structural Analysis, Escuela Técnca Superior de Ingeniería, University of Sevilla, Camino de los Descubrimientos, Sevilla 41092, Spain

[b] Department of Technical Fundamentals of Architectural Design, Faculty of Architecture, Gdańsk University of Technology, Narutowicza 11/12, 80-233, Gdańsk, Poland

[c] Department of Mechanics of Materials and Structures, Faculty of Civil and Environmental Engineering, Gdańsk University of Technology, Narutowicza 11/12, 80-233, Gdańsk, Poland

ARTICLE INFO

*Keywords:*
Rammed earth
Sonic tests
Tomography
Anisotropy
Inspection

ABSTRACT

Rammed earth is a traditional construction technique that has recently gained attention because of its benefits from an ecological perspective. The conservation of the existing valuable cultural heritage sites and the quality control of new constructions built with this material require the development and application of practical inspection techniques. This paper explores the application of sonic tests and sonic tomography as practical tools for monitoring the state of conservation of existing structures and the identification of heterogeneities or damaged areas. Two groups of 6 rammed earth specimens were manufactured and tested. The manufacturing process of each group allowed the application of compression loads and the identification of the Sonic Wave Propagation Velocities along directions parallel and perpendicular to the compaction forces during manufacturing. The SWPV were identified for the different paths between 9 measuring points located at two opposite sides of the specimens, leading to up to 6 different planes for each specimen. The SWPV are identified by identifying the Time-of-Flight of the elastic wave between each pair of excitation and receiver points. A discretized coloured map of the SWPV distribution for each plane defined by the measurement points array is obtained by the application of an algorithm already developed by the authors to obtain tomographic images for other materials and applications. The SWPV are identified after 2 different increasing values of a uniform compressive load is applied to each specimen. The results show that the analysis of the SWPV and tomographic images is sensitive to heterogeneities, such as compaction gradients from the manufacturing process, and also to the accumulated damage in the solid. The paper demonstrates that the proposed technique can be potentially used for a qualitative inspection of the state of conservation of specific rammed earth constructions.

## 1. Introduction

Earth construction is one of the most ancient and worldwide spread building technique. For this reason, a vast amount of valuable earthen heritage sites and historical buildings exist all around the world. However, since its use has almost disappeared in high-income areas of the world, this material has not attracted the attention of researchers until few years ago. One reason for the increasing interest in this material from the academy, is that the development of scientific knowledge is still necessary for dealing with the conservation of earthen heritage sites. Another reason is the concern about the necessary reduction of $CO_2$ emissions from the construction industry. It is estimated that 40% of the total $CO_2$ emissions in the world comes from the cement-based construction industry. Earthen construction provides an attractive eco-friendly alternative to more structurally efficient but ecologically harmful building materials.

Among the different construction techniques that use raw earth as a building material, rammed earth is one of the most widespread and well-known. As with any earth-based construction technique, it requires a suitable composition of the soil (portions of clay, silt, sand and gravel) and a suitable moisture content (typically in the range 8%–15%). Rammed earth walls are built by pouring the humid earth into a mould and compacting it until it is stiff enough. Traditionally, the compaction process is performed manually by using a wooden rammer. A qualitative criterion based on the sound of the impacts is used to determine a sufficient compaction level. The material is poured and compacted in layers (typically 5–15 cm thick). The moisture content is

* Corresponding author.
*E-mail address:* msolis@us.es (M. Solís).

https://doi.org/10.1016/j.engstruct.2024.118058
Received 29 November 2023; Received in revised form 29 February 2024; Accepted 14 April 2024
Available online 23 April 2024

small enough to make the compacted earth stable, so the mould can be immediately removed after compaction of several layers and be placed at another position of the wall to subsequently manufacture additional layers. The external appearance of rammed earth walls is indeed clearly characterized by the identification of the compaction layers.

There are many examples of medium and large size residential buildings, fortresses and defence walls made of rammed earth around the world. Some very well known examples of heritage sites can be found in China (the Big Wall, traditional residential buildings called *tulou*, etc.), Spain (walls of the Alhambra Palace, etc.), Peru (walls of the Chan-Chan city, etc.) and many other countries [1]. Nowadays, rammed earth is probably the most competitive earthen building technique. The main drawback of this technique is that it is very labour intensive when the compaction process is made manually. In modern architecture, however, the compaction is performed by automatic compactors. As a result, the building process is much faster and more efficient. The automatic compaction level can be also higher than the traditional one, making the walls to be more resistant. The mechanical properties of rammed earth are also very good when compared to other earthen building techniques. However, the strength is much lower than other common building materials. The mechanical properties can be enhanced by adding additional binders that combine their effect with the natural effect of the clay in the soil. Rammed earth walls are called stabilized or unstabilized depending on whether or not additional binders are used. Lime is a traditional binder that has been used since ancient times, whereas cement has also been used in the last decades. However, the use of cement reduces the environmental benefits of rammed earth. One of the main research topics related to the use of rammed earth is the study of new eco-friendly binders containing natural materials (biopolymers, etc.) or industrial waste (fly-ash, recycled coarse aggregates, etc.) [2], which make rammed earth more attractive from an ecological and structural point of view.

A relevant challenge for the development of conservation and quality control criteria for rammed earth constructions is the application of non-destructive inspection techniques that can provide information on potentially damaged areas, wall heterogeneity, etc. The scientific community has mainly explored the application of Ultrasonic Pulse Velocity (UPV) identification and the Rebound Hammer (RH) test. The application of these techniques as a practical tool for the estimation of the compressive strength has been studied by several authors [3–6]. The relationship between UPV and other physical parameters such as density and porosity has also been analysed in [3] although no general conclusions could be drawn. The combined application of UPV and RH has been also been considered in [4,6] for the estimation of the compressive strength. In these works, it has been generally observed that higher UPV values are obtained for higher compressive strength. Some regression analysis has also been carried out in order to provide some mathematical expressions that could be used to estimate the compressive strength from UPV and RH values, either alone or combined using a single or multivariate analysis. However, these relationships are obtained for a set of specific rammed earth samples with different soil compositions, additives, etc. As a result, in practice, similar UPV or RH values could be obtained for different rammed earth walls, which may have very different values of the compressive strength due to different physical properties or manufacturing. In other words, such an approach could be useful in practice if a prior calibration of the mathematical correlations is obtained under laboratory conditions for similar rammed earth samples.

Although the application of UPV and RH inspection is well-established in practice for the estimation of the compressive strength of other construction materials such as concrete, the UPV depends directly on the elastic properties of the material (Young modulus and Poisson's ratio for isotropic materials) and not on the compressive strength. The relationship between stiffness and UPV was addressed in [7] where a good correlation was found between the UPV estimate and that obtained by updating a finite element model of a rammed earth wall using modal analysis. However, the value of the Poisson's ratio was first selected by considering the value providing the smallest deviation in terms of natural frequencies. In practice, therefore, the estimation of the Young modulus from UPV values in practice would be affected by the uncertainty in the actual value of the Poisson's ratio.

Sonic testing is another non-destructive inspection technique that is based on the phenomena of elastic wave propagation and wave velocities. In a typical ultrasound test, the excitation is a controlled-frequency wave packet or controlled-width pulse delivered by ultrasound transducers. In contrast, an instrumented impact hammer is usually used for the excitation in the sonic tests. The response is measured at specific points by traditional accelerometers that register wave propagation time histories. The Time of Flight (ToF) of the elastic wave from the source of the excitation to the receiver is determined from the analysis of the recordings from the impact hammer and the accelerometers. The Sonic Wave Propagation Velocity (SWPV) is then determined by just dividing the distance between the excitation and receiver points and the ToF.

Sonic tests have been originally developed and used to inspect other construction materials, mainly masonry walls [8–14]. Few studies have investigated the application of sonic testing to earthen structures [15,16]. In [15] direct sonic tests were used at only 4 locations of a rammed earth wall to evaluate the agreement between the elastic modulus estimated from these tests and from a compression test on samples of the same material. However, the agreement was achieved by finding a proper value of the Poisson ratio. The work presented in [16] is more specifically dedicated to the study of the feasibility of sonic tests as a non-destructive testing technique for the inspection of rammed earth structures. It compares the performance of sonic and ultrasonic tests and demonstrates how sonic tests are a more powerful approach for practical applications in earthen constructions. Because of the typical thickness values of earthen walls, the ultrasonic tests might not be possible to be performed because of the higher attenuation of the ultrasonic waves. This effect becomes more significant when there is accumulated damage due to the loading history of the structure.

As described above, previous applications of sonic and ultrasonic tests have been focused on the estimation of mechanical properties based on elastic wave velocities or the study of their relationship with physical and mechanical properties. However, the application of these techniques to the assessment of heterogeneities in specific rammed earth samples has not been sufficiently explored yet. These heterogeneities may be due to different material properties resulting from a different manufacturing process (different soil composition, additives, compaction energy, moisture, etc.), defects or damage induced by mechanical loads. It is necessary to study the application of these techniques from this perspective. One of the motivations for inspecting real structures by non-destructive tests is to assess their state of preservation and to identify potentially damaged areas. These goals can be addressed by a qualitative analysis of the map of wave velocities at different points and different directions. A single analysis of this type at a specific time can be used to identify possible heterogeneities. Monitoring or comparing the results obtained at different times can provide information on the evolution of damage. A decrease in the identified UPV or SWPV might indicate the appearance or evolution of damage. This qualitative concept is applied in the present paper, being damage or heterogeneity quantification out of the scope of this work.

In a pioneering work of the authors [16], a compaction gradient was identified by a qualitative analysis of UPV and SWPV from top to bottom of some rammed earth specimens. The present work presents an extension of the research described in [16], including results from additional rammed earth samples and exploring the application of sonic tomography to these specimens. The sonic tomography is aimed at obtaining a SWPV map inside the specimen by identifying and combining the SWPV data in different directions, taking into account different positions of source and receiver on the surface of the specimen. Tomographic approaches are widely used in different disciplines

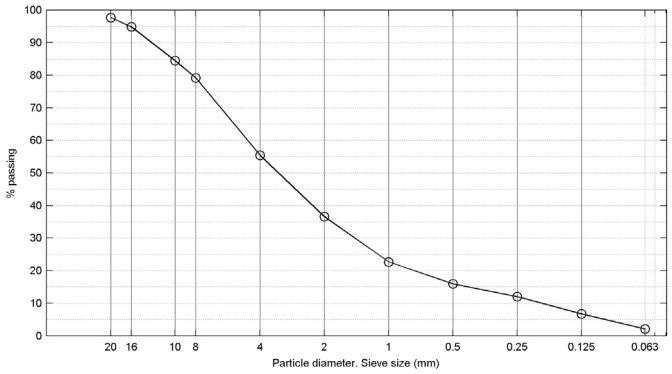


**Fig. 1.** Particle size distribution of selected soil.

for the inspection of solids (medicine, archaeology, geophysics, etc.) using different types of penetrating waves (X-rays, electric fields, magnetic induction, ultrasonic waves, etc.). The application of tomography for the inspection of various materials and structures based on the propagation of elastic waves has been studied [8,17,18]. However, its application to earthen materials has not yet been investigated.

The present paper is organized as follows. First, it includes a description of the specimens (soil properties and manufacturing process) and the procedures for each kind of test (sonic, tomography and compression). Then, the results obtained from the identified SWPV are presented. By analysing the SWPV obtained for different directions, the anisotropic nature of the rammed earth samples is analysed. The study of the SWPV at different locations of the specimens is used for the identification of compaction gradients and the damage extension due to the application of increasing compressive loads. This study is performed based on sonic transmission tomography approach. Finally, conclusions are drawn and future developments are proposed.

## 2. Materials and methods

### 2.1. Soil properties and manufacturing process

The selected soil was employed in a real rammed earth construction site in Valverde del Burguillo (Spain). The construction was performed within the European Project 'LearnBION - Learn Building Impact Zero Network' [19]. The soil was selected from locally available materials by experienced architects and constructors that were involved in the LearnBI0N project. Fig. 1 shows the particle size distribution of the selected soil [20]. According to the Unified Soil Classification System, the soil can be classified as fine to coarse sand (SW). The Liquid and Plastic Limits are 30% and 18% respectively [21].

Twelve specimens were manufactured following traditional techniques. The manufacturing process was supervised by a local expert in rammed earth construction. Two different specimen geometries were used. Their dimensions (height × width × depth) were [600 × 300 × 300] $mm^3$ and [300 × 600 × 300] $mm^3$. They will be referred hereinafter as 'Vertical' (V) and 'Horizontal' (H) specimens, respectively (Fig. 2). The compaction direction was parallel to the largest dimension for the Vertical specimens and to one of the shortest dimensions for the Horizontal ones. For each layer, a certain amount of moist soil was poured into the wooden mould and a controlled compaction energy was applied and distributed manually for each layer. By controlling the number of impacts and the drop height of the rammer, a compaction energy of 364 $kJ/m^3$ was applied as uniformly as possible for each layer. The thickness of each layer was approximately 75 mm, so a total of 8 and 4 layers were compacted for the Vertical and Horizontal specimens, respectively. Based on the obtained Optimum Moisture Content obtained from a Standard Proctor Test, the moisture content during manufacturing was 5.1%. This is relatively a low value for rammed earth, maybe due to a low presence of silt and clay in the selected soil. This could also explain the relatively low compressive strength obtained for the specimens, as detailed in next section. The mean value of the dry density of the specimens after manufacturing was 1928 $kg/m^3$. More details and discussion about the different parameters involved in the manufacturing process can be found in a previous related work [16].

### 2.2. Compression tests

Simple compression tests were performed for each specimen. Two different loading directions with respect to the compaction direction were considered. The compressive load was applied parallel and perpendicular to the compaction direction for the Vertical and Horizontal specimens, respectively. The loading direction was parallel to the longest dimension of the specimens, in order to ensure a slenderness of 2 for the compression tests. Since the loading frame allowed only a vertical loading direction, the Horizontal specimens had to be turned upside down 90 degrees. A servohydraulic actuator was used and the tests were displacement-controlled at 3 mm/min rate. A gypsum layer was placed in between the upper and lower sides of the specimens and the platens of the testing machine (Fig. 2(d)). These layers were introduced in order to mitigate the effect of irregularities of the contact surfaces and to allow a uniform load distribution.

The tests were not designed in order to obtain an accurate characterization of the compressive strength of the material by following recommendations from reference Standards, but to generate progressive damage on the specimens and study its effect on the results from sonic tests. Loading and unloading cycles were carried out in order to characterize the velocity of sonic wave propagation after different load levels (referred as Load 0, Load 1 and Load 2 hereinafter) had been applied to the specimens. As a result, the effect of the different damage states on the inspection by sonic tests can be analysed. In order to analyse the effect of similar expected damage on the different specimens, similar load levels, defined as a percentage of the compressive strength of each specimen, should be applied. However, this could not be achieved because of the variation of strength between different specimens, so it is unknown in advance for each specimen. Thus, different load levels were applied during the experimental campaign, considering preceding obtained values and expectations for each specimen. Table 1 includes the final load levels considered for each loading cycle, also expressed as a percentage of the finally obtained compressive strength, and the value of the final compressive strength for each specimen. These estimated values of the compressive strength should be, however, considered with caution because they could be affected by the different loading procedure followed for different specimens and the absence of a reference methodological procedure based on commonly used Standards.

### 2.3. Sonic tests

As the source of the elastic waves, an impact hammer of 11 mV/N sensitivity with a hard tip was used (model 056C01 from PCB company). The receiver sensors were nine piezoelectric accelerometers of 100 mV/g sensitivity (model 256HX-100 from Endevco company). The accelerometers were fixed to one side of the specimens by attaching them to a metal base, which was previously glued to the specimen with wax. A LAN-XI dynamic analyzer module (from Brüel and Kjaer) was used for the data acquisition. The sampling rate was set the at maximum available frequency (65 536 Hz). For the determination of the SWPV between the excitation and the receiver points, 30 impacts were applied and recorded independently at each excitation point. The SWPV for each path connecting the excitation point and each receiver point was determined by the identification of the ToF of the elastic wave between both points. The SWPV was evaluated as the distance

(a)

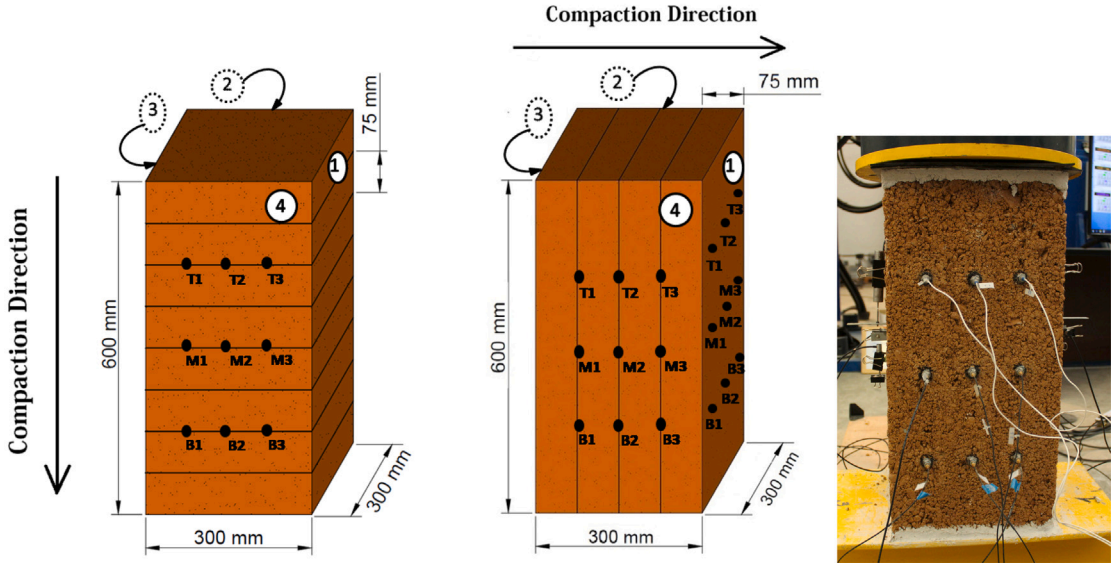


(b) (c) (d)

**Fig. 2.** (a) Specimens on their position after manufacturing. (b,c) Dimensions, sides numbers, and measuring points of vertical (b) and horizontal (c) specimens at their position during the compression and sonic tests. (d) Picture of the experimental set-up.

**Table 1**
Load values of each loading–unloading cycles, compressive strength ($f_c$) of each specimen.

| Specimen | V1 | V2 | V3 | V4 | V5 | V6 |
|---|---|---|---|---|---|---|
| 1st load [MPa], (%$f_c$) | 0.40 (38) | 0.40 (52) | 0.40 (53) | 0.40 (63) | 0.40 (53) | 0.40 (39) |
| 2nd load [MPa], (%$f_c$) | 0.80 (75) | – | – | 0.55 (86) | 0.55 (73) | 0.8 (78) |
| $f_c$ [MPa] | 1.06 | 0.77 | 0.75 | 0.64 | 0.75 | 1.03 |
| Specimen | H1 | H2 | H3 | H4 | H5 | H6 |
| 1st load [MPa], (%$f_c$) | 0.33 (85) | 0.13 (30) | 0.13 (33) | 0.13 (43) | 0.13 (29) | 0.33 (100) |
| 2nd load [MPa], (%$f_c$) | – | – | 0.27 (68) | 0.27 (90) | 0.27 (60) | – |
| $f_c$ [MPa] | 0.39 | 0.44 | 0.40 | 0.30 | 0.45 | 0.33 |

between each pair excitation-receiver points divided by the ToF. For the determination of the ToF, an automated and calibrated algorithm developed by the authors is applied [16].

The sonic tests were performed before any load was applied on each specimen and after the loading–unloading cycles were applied as explained in the compression tests description. Nine measurement points were distributed in a Top row (T1, T2, T3), Middle row (M1, M2, M3) and Bottom row (B1, B2, B3) as illustrated in Fig. 2(b) and (c). The excitation points were located in front of the receiver points at the opposite side. The SWPV between each point on the excitation face and the 9 reception points on the opposite face were determined. Even though measuring points seem to be located precisely at layer interfaces in Fig. 2(b) and (c), it must be noted that layer heights after manufacturing were not precisely 75 mm, the size of the accelerometers base is relatively big (15 mm diameter) and location of manual impacts have an implicit uncertainty in their precise location. As a result, it

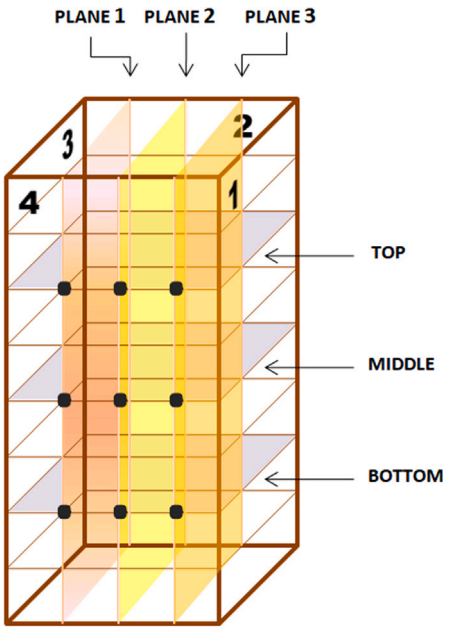


**Fig. 3.** Planes defined for tomography.

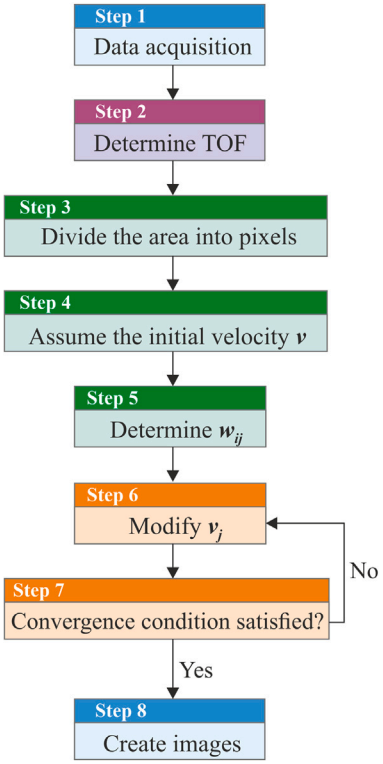


**Fig. 4.** Flowchart of ultrasonic tomography algorithm.

cannot be considered that measuring points are located at interfaces. The study of the possible influence of the precise locations of measuring points within a specific layer would require a detailed experimental configuration and a specific analysis that is out of the scope of the present work.

For the analysis of the evolution of the SWPV during the loading–unloading cycles in the horizontal specimens, the impacts perpendicular to the compaction direction (from side 2 to side 4) were considered for both the Vertical and Horizontal specimens. However, for the latter, an additional arrangement of excitation and receiver points (at sides 1 and 3) was considered when no load was applied yet. The results from these two different arrangements allow the determination and comparison of the SWPV when the excitation impact is perpendicular or parallel to the compaction direction.

### 2.4. Tomography

Transmission tomography based on elastic wave propagation is a widely used method of non-destructive testing. It allows the reconstruction of the internal structure of the tested object based on the information obtained from the acoustic wave propagating through the tested element. The method allows the determination of the elastic wave velocity distribution, which depends on the homogeneity and quality of the tested material. The velocity distribution can be used to assess voids, compaction, or stratification in the soil. In this work the 3D analysis is performed by reconstruction the information for 6 different planes (3 vertical and 3 horizontal), as defined in Fig. 3.

The information used in the image reconstruction procedure for rammed earth samples is the ToF. The flowchart of sonic tomography is shown in Fig. 4. The procedure starts with data acquisition of the elastic waves passing through the specimen from the transmitters to the receivers (Figs. 4 and 5, step 1) and the determination of the time of flight for each wave (Figs. 4 and 5, step 2). To determine the velocity distribution in the section under test, the element is divided into small elements called pixels (Figs. 4 and 5, steps 3–5). Each pixel is assigned a specific, constant value of the wave propagation velocity.

The ToF of the $i$th ray of the propagating wave from the transmitter to the receiver can be expressed as:

$$t_i = \sum_{j=1}^{n} w_{ij} \frac{1}{v_j} \qquad i = 1, 2, 3, \ldots, m \qquad j = 1, 2, 3..., n \tag{1}$$

where $w_{ij}$ is the length of the $i$th ray passage through the $j$th pixel, $t_i$ is the time of flight of the P-wave propagating between the transmitter and receiver along the $i$th ray, $v_j$ is the velocity in $j$th pixel and $s_j$ is the slowness in $j$th pixel. The choice of the pixel size sonic tomography is closely related to the number of measurement points. In the present study, the distance between the measuring points was 75 mm in the horizontal direction and 150 mm in the vertical direction. Therefore, the pixel size was 75 mm × 75 mm in the horizontal planes and 150 mm × 75 mm in the vertical planes. The rays were traced from a given transmitter to each of the receivers which resulted in m = 9 rays for each of the planes. Nine rays allowed the velocity values to be reconstructed in 15 pixels, which was sufficient to identify the anisotropy and compaction gradient of the rammed earth samples. It should be noted that the total number of pixels was $n = 25$, but only $n = 15$ were active, because rays only passed through 15 pixels, as the points are on a pair of opposite edges.

Measurements of all the propagating wave paths from the transmitters to the receivers produce a system of equations with known values for the times of flight (matrix **t**) and the lengths of the paths passing through the pixels (matrix **w**), and with the unknown value of the slowness in individual pixels, according to the equation:

$$\mathbf{t}_{mx1} = \mathbf{w}_{mxn}\mathbf{s}_{nx1} \tag{2}$$

The main purpose of sonic tomography is to calculate the slowness matrix **s**. It is worth noting that the path $j$ propagating from the transmitter to the receiver crosses only a few pixels, leaving the others out. Therefore, most of the values in the **w** matrix are equal to zero. However, it is an ill-posed and sparse matrix (many rows are linearly related and most row elements are zero). This leads to ambiguity in the solutions. Commonly used methods such as Gaussian elimination, matrix inversion, and least squares cannot be used. Furthermore, a small error in the measurement or interpretation of the results can have a significant impact on the final image reconstruction result. Special solution methods have to be used. Most techniques for solving Eq. (2)

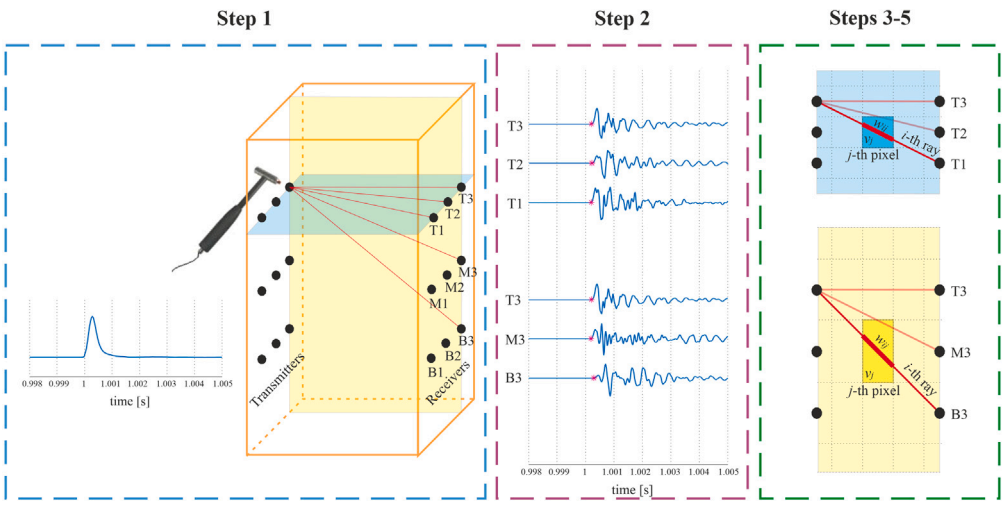


**Fig. 5.** Illustration of steps 1–5 of tomography algorithm.

are based on specific iterative methods. One of these is the Algebraic Reconstruction Technique (ART), which updates the solution by successively processing each equation separately until the convergence condition is reached. In the first step, each pixel has the same value of the wave propagation velocity, assuming that the tested cross-section is homogeneous. In this case, elastic waves propagate along straight lines (Fig. 5). Then the iteration process begins, which can be described mathematically by the formula [22]:

$$s_j^{(k)} = s_j^{(k-1)} + \frac{w_{ij}\Delta t_i}{\sum_{j=1}^{n} w_{ij}^2} \tag{3}$$

where $\Delta t_i$ is the difference between the original projection time and the reconstruction time.

The image reconstruction scheme of the tested rammed earth specimens is shown in Fig. 6. In the first step, the image for each tested plane is made independently, and each pixel is assigned a value. Then the images for the planes are blurred.

## 3. Experimental results and discussion

### 3.1. Anisotropy assessment

The sonic tests performed for the Horizontal specimens, by means of impacts in the parallel and perpendicular directions to the direction of compaction, allow the determination of SWPV for both directions. Fig. 7 shows the SWPV determined at each measuring point when the excitation source is located just in front of it, obtained for the two directions. The average and standard deviation of this set of values for each specimen is represented in Fig. 8. It shows that noticeable variations can be observed between different specimens, but values for each direction are similar for each specimen (with the only exception of specimen H6 for which no reason is found to explain this abnormal result). Table 2 shows the level of confidence obtained from T-Student tests performed for SWPV values along the two directions for each specimen. A very low confidence level is only obtained for specimen H6. The values obtained for the rest of the specimens support the hypothesis that the average values of SWPV for both directions are unlikely to be significantly different, even though the confidence interval indicates that there is a higher probability of finding greater values of SWPV for the compaction direction. Considering the scattering of the results for both directions and the different relative values of SWPV for specimens (bigger or smaller values for any of the two directions are found), the assumption of expecting similar SWPV values for both directions can be considered a reasonable hypothesis in practice.

In addition, Fig. 8 shows that higher SWPV values, identified along any direction, are found for specimens with higher mechanical strength. This observation is in agreement with the results presented in [3,5,6].

Results from Table 1 also show that the compressive strength of the Horizontal specimens was lower than that of the Vertical ones. Since the propagation of the elastic waves is actually related to the material stiffness and density and not to the strength, a possible explanation for this phenomenon is that the material exhibits similar stiffness along the directions parallel and perpendicular to the compaction layers, but the compressive strength might be different when the load is applied at those two different directions. One explanation for this phenomenon is the failure mode of Horizontal specimens induced by separation of the compaction layers during compression due to indirect tensile strains along the direction perpendicular to compaction. Fig. 9 illustrates the difference between the usual failure mode of Vertical and Horizontal specimens. For the first, a smeared cracking is observed at the external surface of the specimens. In contrast, for the latter, vertical cracks due to separation between compaction layers are observed. In addition, for this specific experimental campaign, the compressive tests of Horizontal specimens might be affected by the geometric irregularities of the top surface during the manufacturing process (side 3 in Fig. 2(c)). The lack of flatness of this side make the cross-section of the Horizontal specimens during the compression tests not to be strictly constant and this phenomenon might lead to localized cross-section reductions and non-uniform stress distributions, affecting the global compressive strength of the specimen. A non-uniform load distribution can also be induced by different stiffness of the layers due to compaction gradients, as they are identified in next section.

The analysis and quantification of the anisotropic nature of rammed earth has not sufficiently addressed yet in the literature. One possible reason for this is the difficulty in manufacturing slender specimens to be loaded in the perpendicular direction to compaction (parallel to the layers). The authors are only aware of one related specific work [23]. It shows that rammed earth can be considered an isotropic material in terms of stiffness and compressive strength. However, it also remarks that this isotropic behaviour requires a perfect adherence between the compaction layers. If separation takes place, then a different behaviour might be observed along the parallel and perpendicular direction to the layers. Thus, even though a perfect adherence can be assumed at an initial stage based on the isotropic nature of the identified SWPV at Load 0, a failure mode due to separation of the layers during compression could also explain the difference in the compressive strength observed for the Horizontal and Vertical specimens in the present work.

In a previous work [3], it was also observed that similar ultrasonic wave propagation velocities were obtained in any direction of rammed

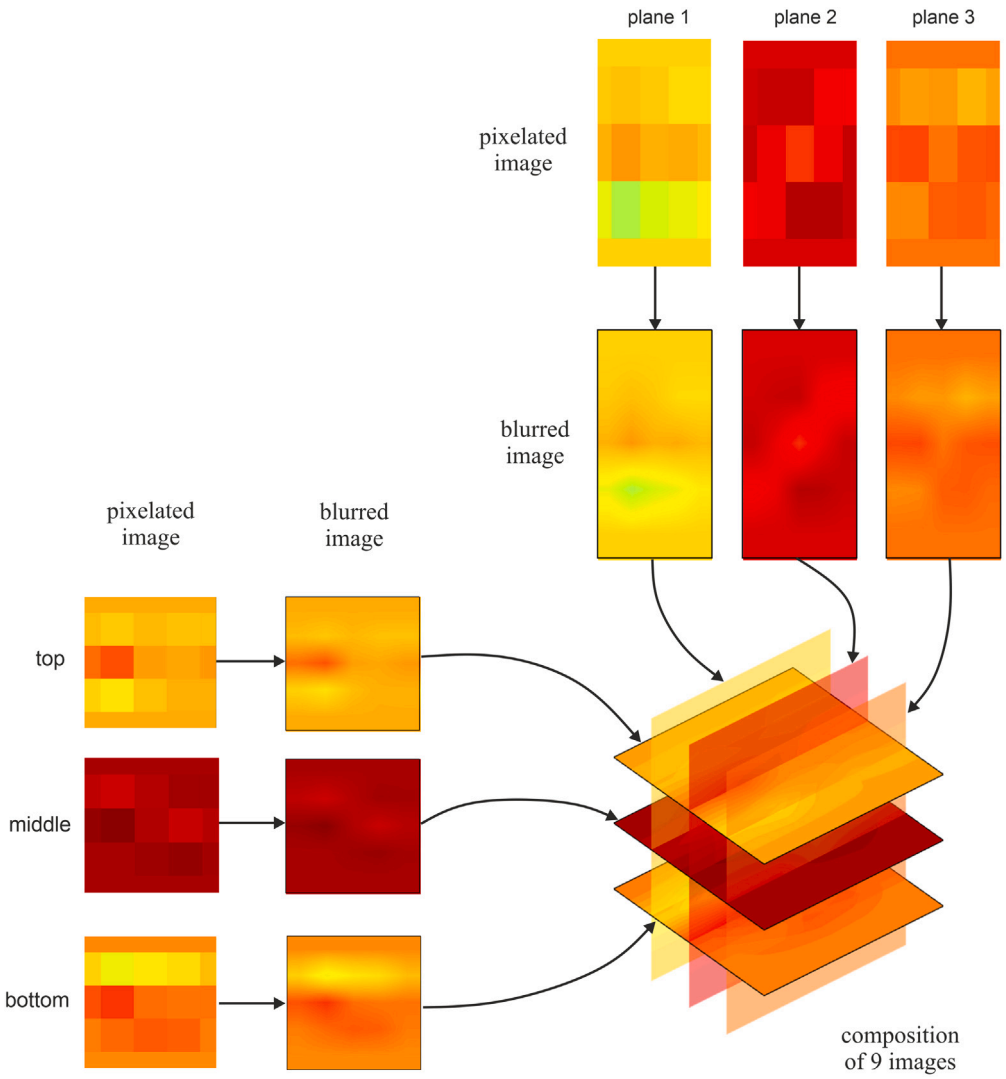


**Fig. 6.** Image generation scheme.

**Table 2**
Level of confidence (p) and 95% confidence interval (ci) for the difference in average values obtained from T-Student tests between SWPV values for parallel and perpendicular directions to compaction.

| Specimen | H1 | H2 | H3 | H4 | H5 | H6 |
|---|---|---|---|---|---|---|
| p | 0.13 | 0.48 | 0.61 | 0.98 | 0.39 | 0.002 |
| ci | [−43,323] | [−158,325] | [−150,90] | [−276,269] | [−90,218] | [−478,-135] |

earth samples. This observation is consistent with the results presented here. In a different study [24] a small difference in these velocities were obtained for the compaction direction and the perpendicular direction. However, this work analysed the behaviour of small specimens of statically compressed earth. Thus, there were no different compaction layers and the different compaction process could also induce some anisotropic behaviour in the particles arrangement. In the same work, a small difference of about 10% was also obtained for the tensile strength in these two directions.

### 3.2. Compaction gradient and damage sensitivity

Figs. 10 and 11 show, for the Vertical and Horizontal specimens, respectively, the identified SWPV between each excitation point and the corresponding measuring point in front of it at the different load levels. It is recalled here that SWPV are determined between planes 2 and 4 (Fig. 2(b,c)), so the SWPV values correspond to directions perpendicular to compaction direction (NC in Fig. 7) . Some trends can be observed on the results providing practical information about the performance of the inspection technique. First, it is observed that the values of the identified SWPV decrease as the level of the applied load increases. Thus, the SWPV are sensitive to the cumulative damage on the material. This is an interesting result which illustrates that the identification of the SWPV over time can be used to identify potentially damaged areas in real structures during their service life. At this point, it must be noted that the value of the SWPV by itself does not provide information about the conservation state. It is the comparison of the SWPV at a certain position at different times that can be used for this purpose. In addition, not only one measuring point, but the distribution and evolution of the SWPV at different positions should be considered for this kind of analysis.

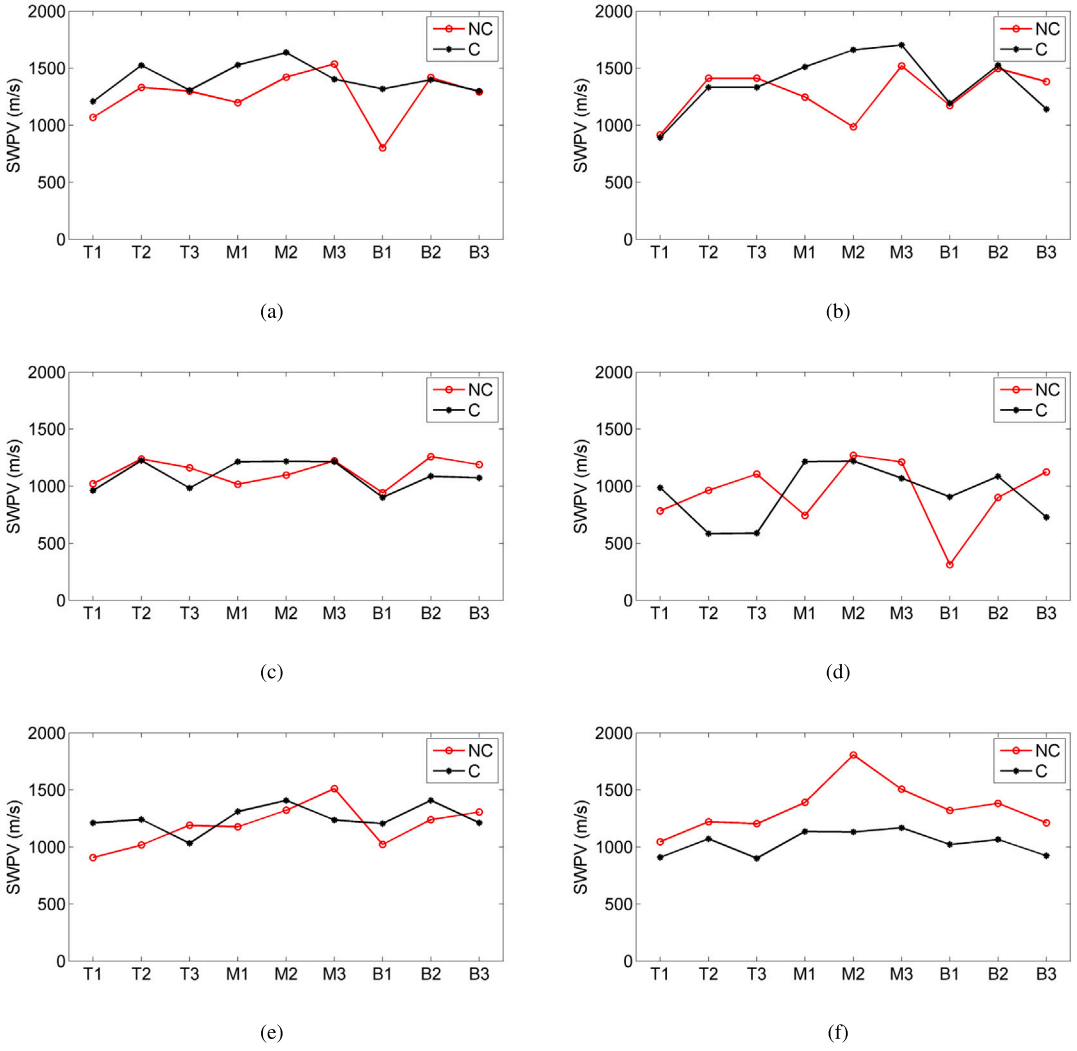


**Fig. 7.** SWPV at Load 0 for each measuring point and directions perpendicular (Non-Compaction, NC) and parallel (Compaction, C) to the compaction direction for specimens (a) H1, (b) H2, (c) H3, (d) H4, (e) H5 and (f) H6.

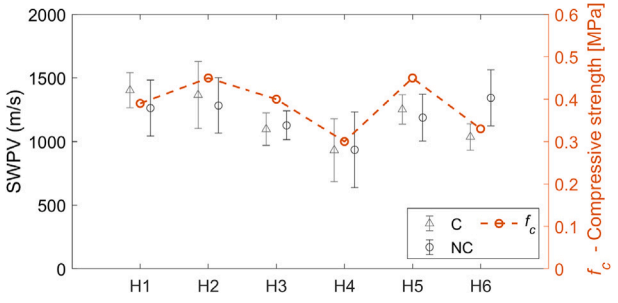


**Fig. 8.** Average (markers) and standard deviation amplitude (vertical lines) of SWPV at Load 0 for directions perpendicular (Non-Compaction, NC) and parallel (Compaction, C) to the compaction direction and compressive strength (fc) for each horizontal specimen.

In addition, the results illustrate how the inspection technique is sensitive to the heterogeneity of the material. Variations in the values of the obtained SWPV are consistent to compaction gradients due to the manufacturing process. Due to the subsequent compaction of layers from bottom to top, the lower layers receive a higher compaction energy. Moreover, despite taking care of applying a uniform distribution of the compaction energy over the top surface of each layer, the central area of the surface usually receives a higher compaction energy since it receives part of the energy that is also applied in the surrounding areas. In addition, less energy is applied in these areas because of the difficulty in impacting with the rammer at areas close to the mould.

As a result, Fig. 10 shows that, in general, a gradient of SWPV is identified from the top to the bottom layers in the Vertical specimens due to the higher compaction of the lower layers. Higher SWPV values are obtained for the measuring points at the bottom row and lower values for the top row. In addition, within each row, a higher SWPV value is obtained at the central points , since the central areas are usually more compacted, as explained above. In the case of the Horizontal specimens (Fig. 11), due to the higher compaction of the lower layers, a gradient is observed from measuring points 1 to 3. On the other hand, due to the higher compaction in the central area of the top surface during manufacturing, higher values are obtained for the middle row of measuring points. However, this second compaction gradient is less clear for the Horizontal than for the Vertical specimens due to the fact that the compaction surface for the Horizontal ones is larger, making it easier to apply a more uniform compaction energy over this surface.

### 3.3. Sonic tomography

Figs. 12–17 and 18–23 show the SWPV maps obtained from the tomography inspection for the Horizontal [H1–H6] and Vertical [V1–V6] specimens, respectively. They include the maps for the three

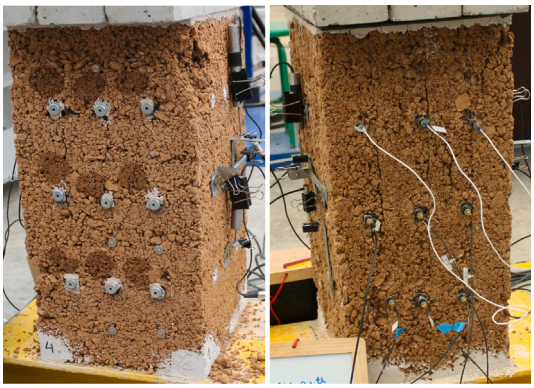

(a) (b)

**Fig. 9.** Illustration of failure modes of (a) Vertical and (b) Horizontal specimens.

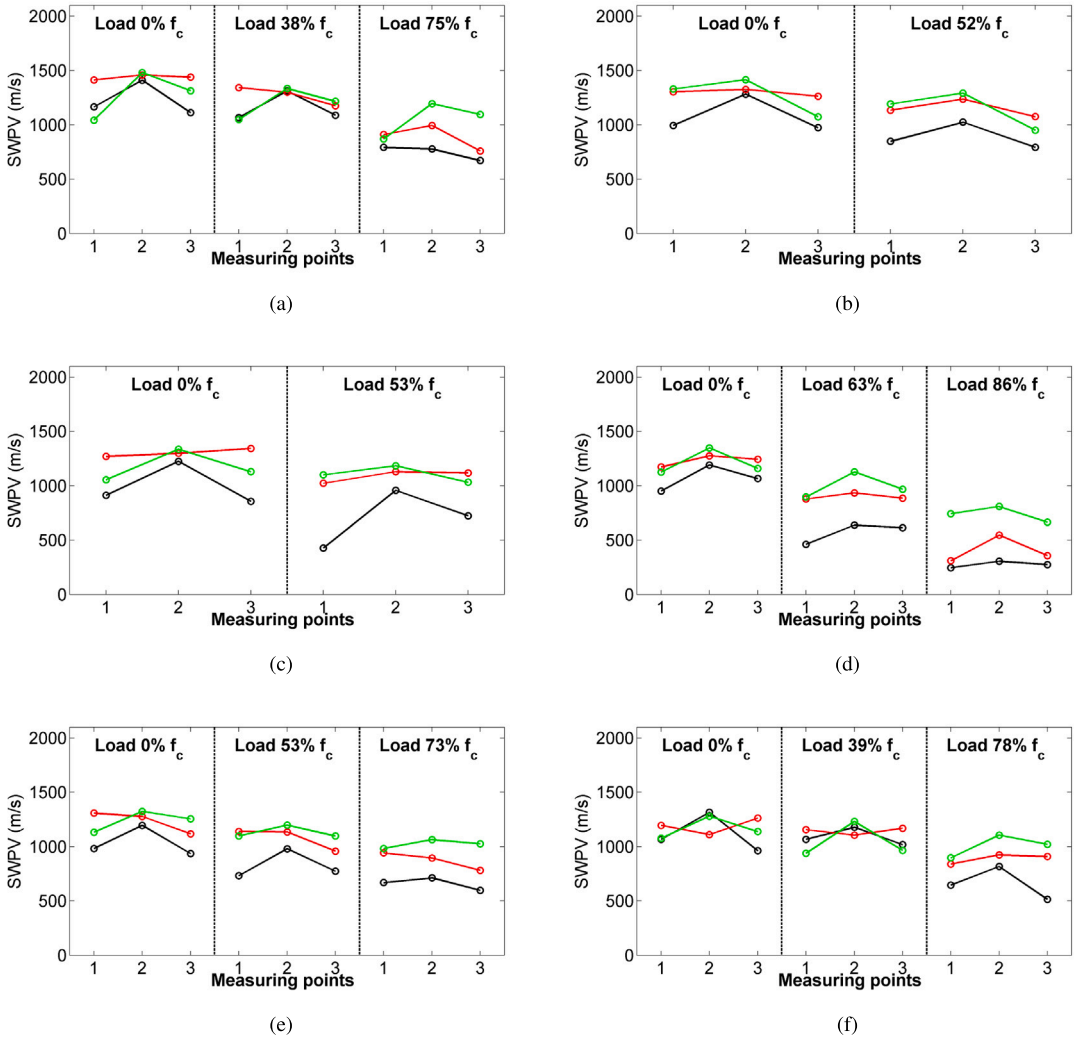


**Fig. 10.** SWPV at Load 0, Load 1 and Load 2, for each measuring point and for Vertical specimens (a) V1, (b) V2, (c) V3, (d) V4, (e) V5 *y* (f) V6. Black, red and green lines correspond to top, middle and bottom rows of measuring points. (For interpretation of the references to colour in this figure legend, the reader is referred to the web version of this article.)

independent horizontal and vertical planes, defined between sides 2 and 4 of the specimens and therefore corresponding to directions perpendicular to compaction direction, (Figs. 2(b,c) and 3) as well as their 3D reconstruction.

It can be observed from the Figs. 12–17 that, for the Horizontal specimens, a SWPV gradient can be observed from plane 1 to plane 3. Due to the effect of the compaction process, higher velocities are observed for the bottom plane during manufacturing (Plane 3). In

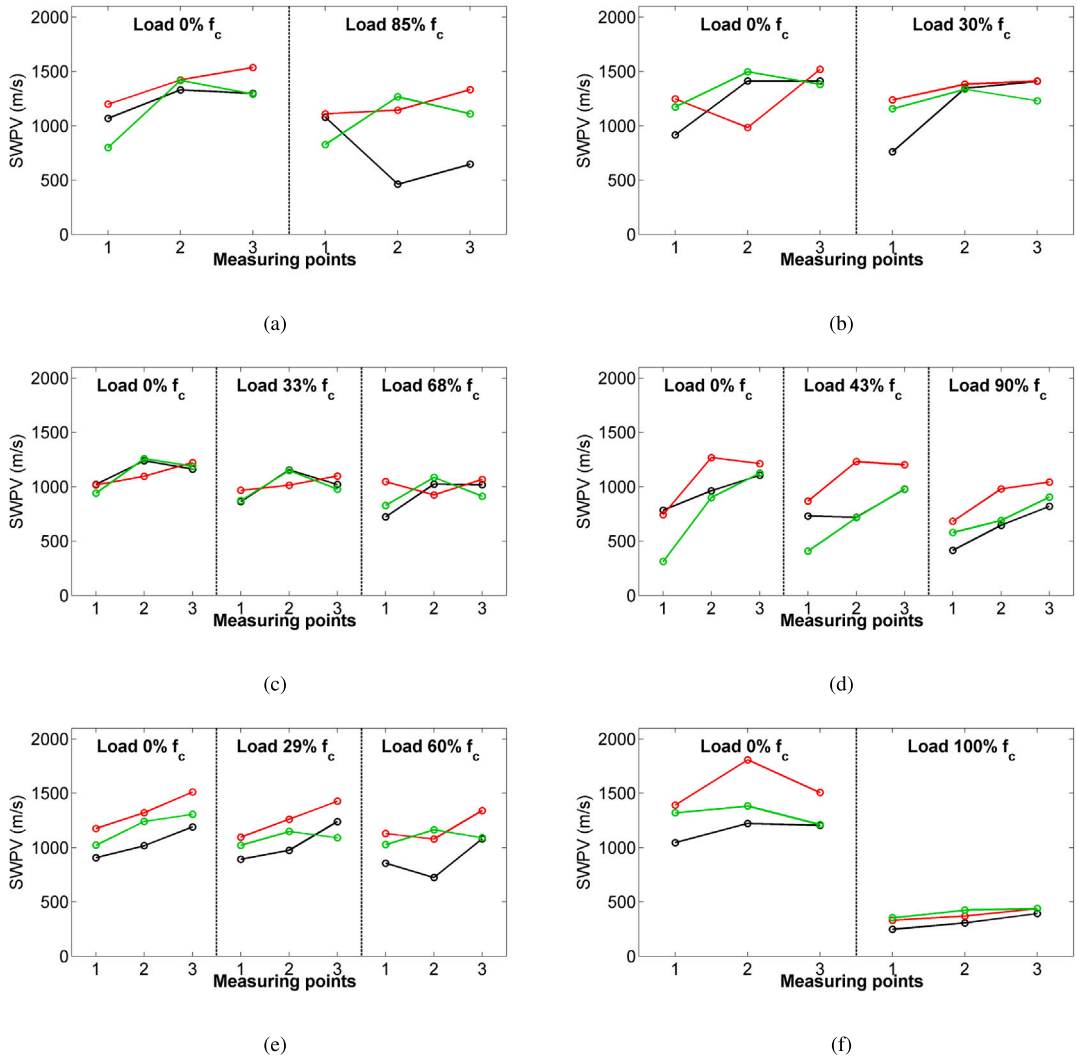


**Fig. 11.** SWPV at Load 0, Load 1 and Load 2, for each measuring point and for horizontal specimens (a) H1, (b) H2, (c) H3, (d) H4, (e) H5 *y* (f) H6. Black, red and green lines correspond to top, middle and bottom rows of measuring points. (For interpretation of the references to colour in this figure legend, the reader is referred to the web version of this article.)

general, the distribution of velocity values in tomographic images was rather uniform at Load 0 on all planes 1–3. Only for specimen H2, local area with a higher velocity appeared on the map for plane 2. In addition, the higher compaction level in the central part of the specimen is illustrated by higher SWPV values at the middle plane.

As the applied load level increased, lower velocities were obtained and potentially damaged areas can be identified from the SWPV maps. Maps began to reveal heterogeneities in velocity distribution for load levels 1 and 2. Areas with lower values of velocity indicated regions with potential damage initiation. In general, this decrease is more significant at vertical plane 1 and horizontal planes located at top and bottom positions, indicating the presence of more significant structural damage in those areas. For specimen H6 and after load 1 is applied (Fig. 17), extremely low velocities are obtained for the whole specimen. As a matter of fact, the specimen failure took place at the same load value as load 1. This result illustrates how low SWPV maps obtained from this inspection technique could indicate that the material has been close to failure and therefore is extremely damaged. The possible lack of adherence between the compaction layers associated with the failure mode of Horizontal specimens, can justify the presence of interfaces that could slow down the wave propagation leading to a decrease in SWPV that is represented by a global decrease in the whole specimen. The existence of these interfaces or delaminations is not detected from sonic tomography maps for none of the specimens for the intermediate damage levels induced. More detailed information from sonic tomography using a higher number on measuring points and pixel resolution can provide information about this phenomenon and the actual sensitivity of this inspection technique.

For the Vertical specimens, the compaction gradient can be identified from the increasing velocities obtained from top to bottom and at the central part of the specimen (plane 2). As the load increased, lower values of SWPV are found at horizontal top plane and vertical planes 1 and 3, indicating the likely existence of more significant damage in those regions. For the specimens that 2 load levels were applied and they were close to the compressive strength, very low SWPV maps are obtained for the whole specimen at the final stage.

## 4. Conclusions

The results from the present work illustrate that the inspection of rammed earth samples by sonic testing is a feasible technique that can provide useful information for a qualitative analysis of heterogeneity due to different compaction levels and cumulative damage.

Similar values of the identified SWPV have been found along perpendicular and parallel directions to the compaction layers. However, different compressive strength values have been found when load is

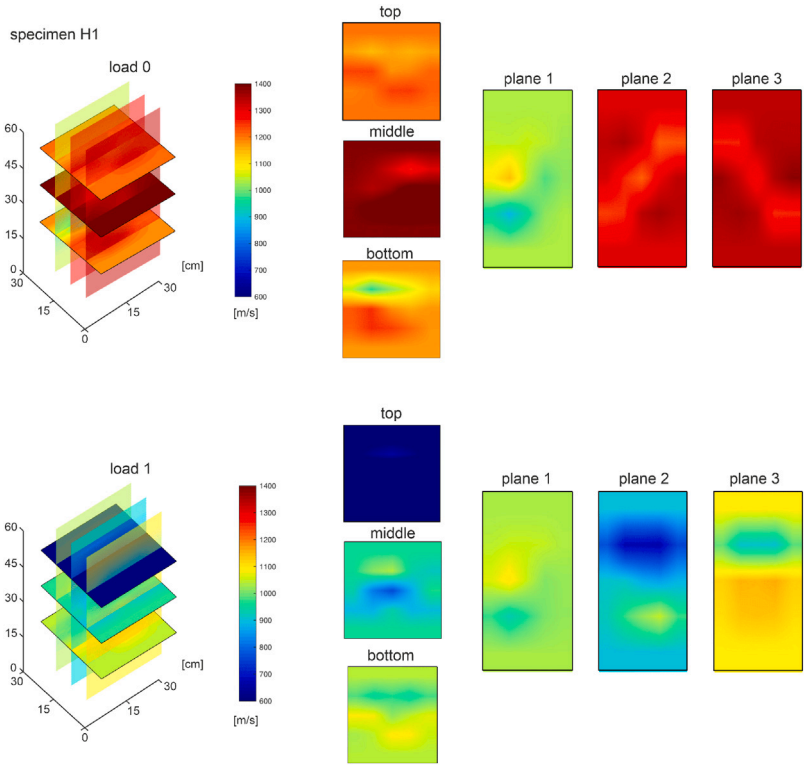


**Fig. 12.** Results from sonic tomography (specimen H1).

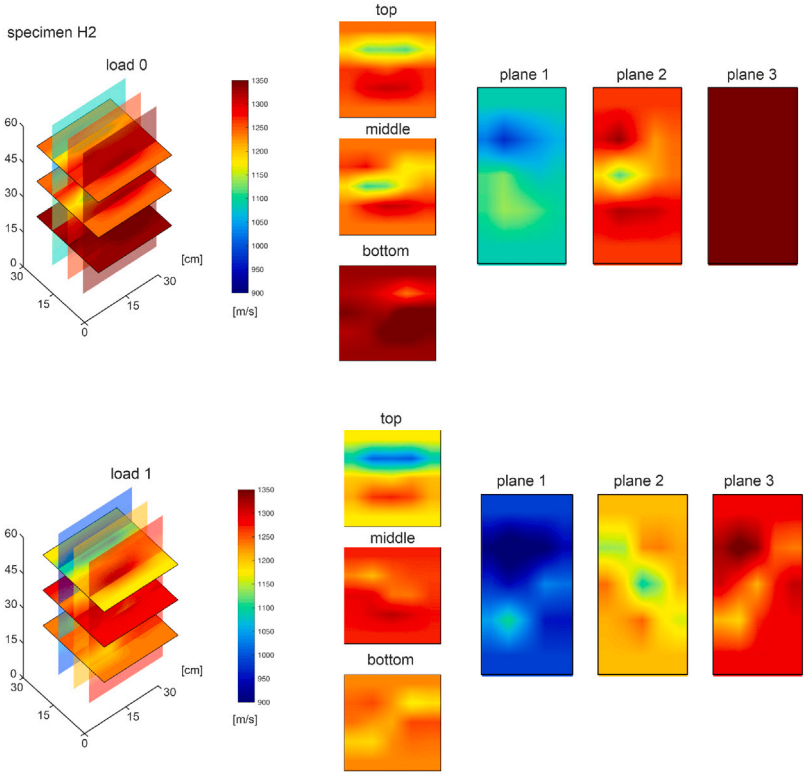


**Fig. 13.** Results from sonic tomography (specimen H2).

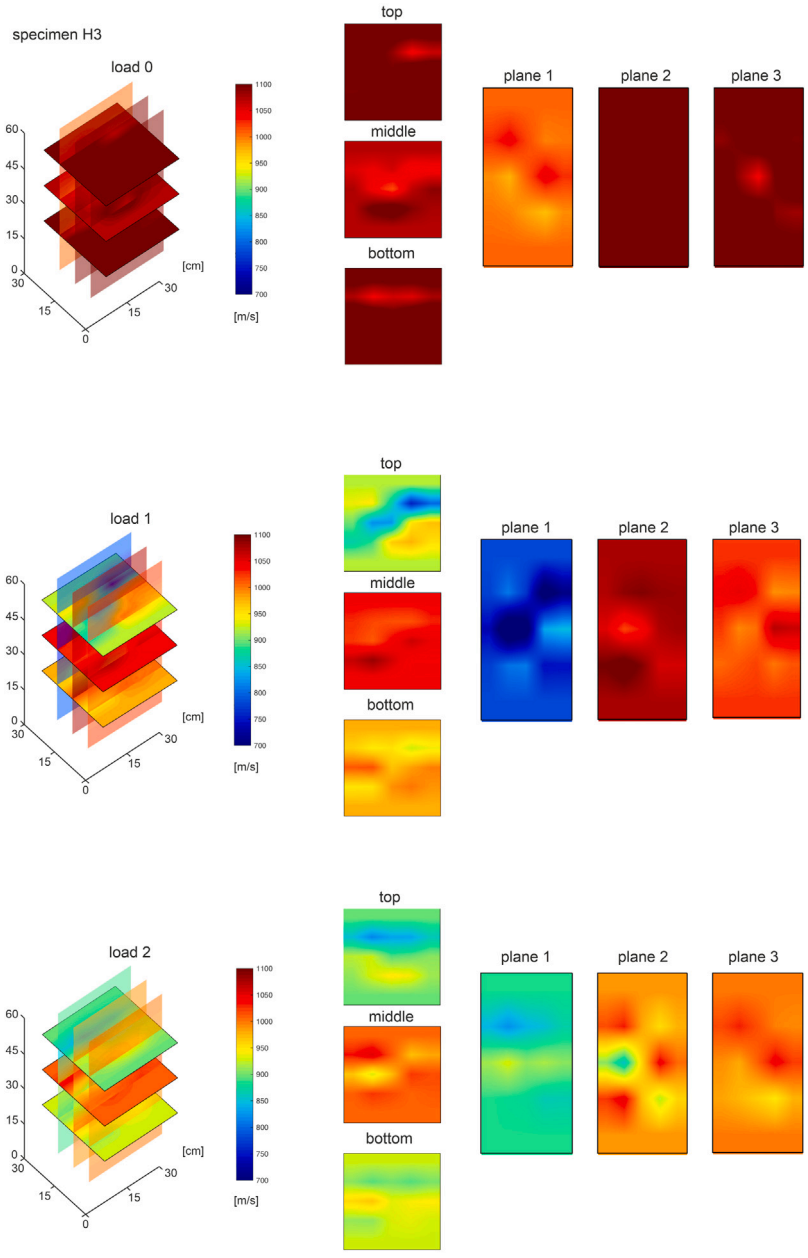


**Fig. 14.** Results from sonic tomography (specimen H3).

applied at both directions. The lower compressive strength obtained for the Horizontal specimens (for which the load is applied in a parallel direction to compaction) could be explained by non-uniform load distribution due to their geometric irregularities from the manufacturing process, different stiffness of the layers (parallel to the loading direction) or a failure mode due to a possible loose of perfect adherence between the compaction layers. Future experimental tests assessing the compressive strength values obtained for specimens with only a single compaction layer could serve for validating or not this hypothesis about the different compressive strength obtained for the horizontal and vertical specimens in this work, despite the similar SWPV obtained for both of them in different directions.

The tomography approach applied in this paper appeared to be an effective technique for the inspection of this building material. In the present work, by using 9 pairs of measurement points located at two opposite sides of the specimen (9 source points and 9 corresponding opposite receiver points), reconstruction of the internal structure of earth specimens was obtained. Tomographic imaging in 2D planes (three vertical planes and three horizontal planes) as well as 3D reconstruction enabled observation of changes wave velocities inside the specimens. Despite a relatively low resolution of the measurement points grid considered in this application, the resulting obtained images of SWPV provided a comprehensive insight of the heterogeneity of the material and potentially damaged areas.

The paper illustrates the feasibility of this technique for a qualitative inspection of rammed earth structures. By comparing SWPV values for a certain specimen, potentially damaged or less stiff areas can be identified. In addition, by monitoring the SWPV values along the service life of the construction, the evolution of potentially damaged patterns can be achieved. A particularly low SWPV values can be used as damage indicators providing an alert of extremely severe damage due to an extreme loading scenario that might have taken place. Damage quantification and the analysis of the sensitivity to early

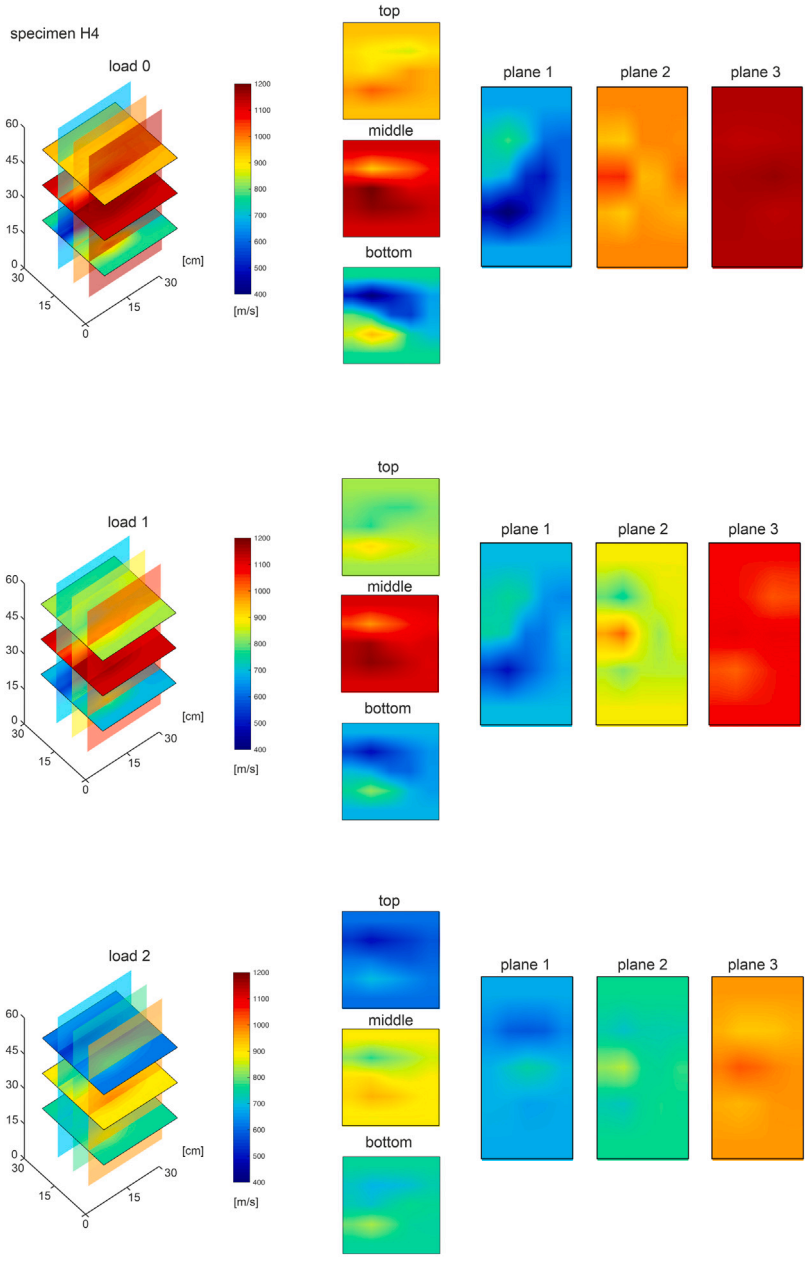


**Fig. 15.** Results from sonic tomography (specimen H4).

damage in practice require further research on this topic. Tomography results from a more dense measurement points grid and for different controlled damage states is considered as a future research work to provide quantitative information about the actual sensitivity of the technique to early damage and its evolution.

## CRediT authorship contribution statement

**J.D. Rodríguez-Mariscal:** Writing – review & editing, Writing – original draft, Investigation, Conceptualization. **M. Zielińska:** Writing – review & editing, Writing – original draft, Visualization, Software, Methodology, Formal analysis. **M. Rucka:** Writing – review & editing, Writing – original draft, Visualization, Software, Methodology, Conceptualization. **M. Solís:** Writing – review & editing, Writing – original draft, Supervision, Methodology, Formal analysis, Conceptualization.

## Declaration of competing interest

The authors declare that they have no known competing financial interests or personal relationships that could have appeared to influence the work reported in this paper.

## Data availability

Data will be made available on request.

## Acknowledgements

The authors would like to acknowledge the financial support provided by the Spanish Ministry of Science, Innovation and Universities, Spain (research project PID2019-109622RB) and the Regional Ministry of Economic Transformation, Industry, Knowledge and Universities of Andalusia, Spain (research project PROYEXCEL_00659).

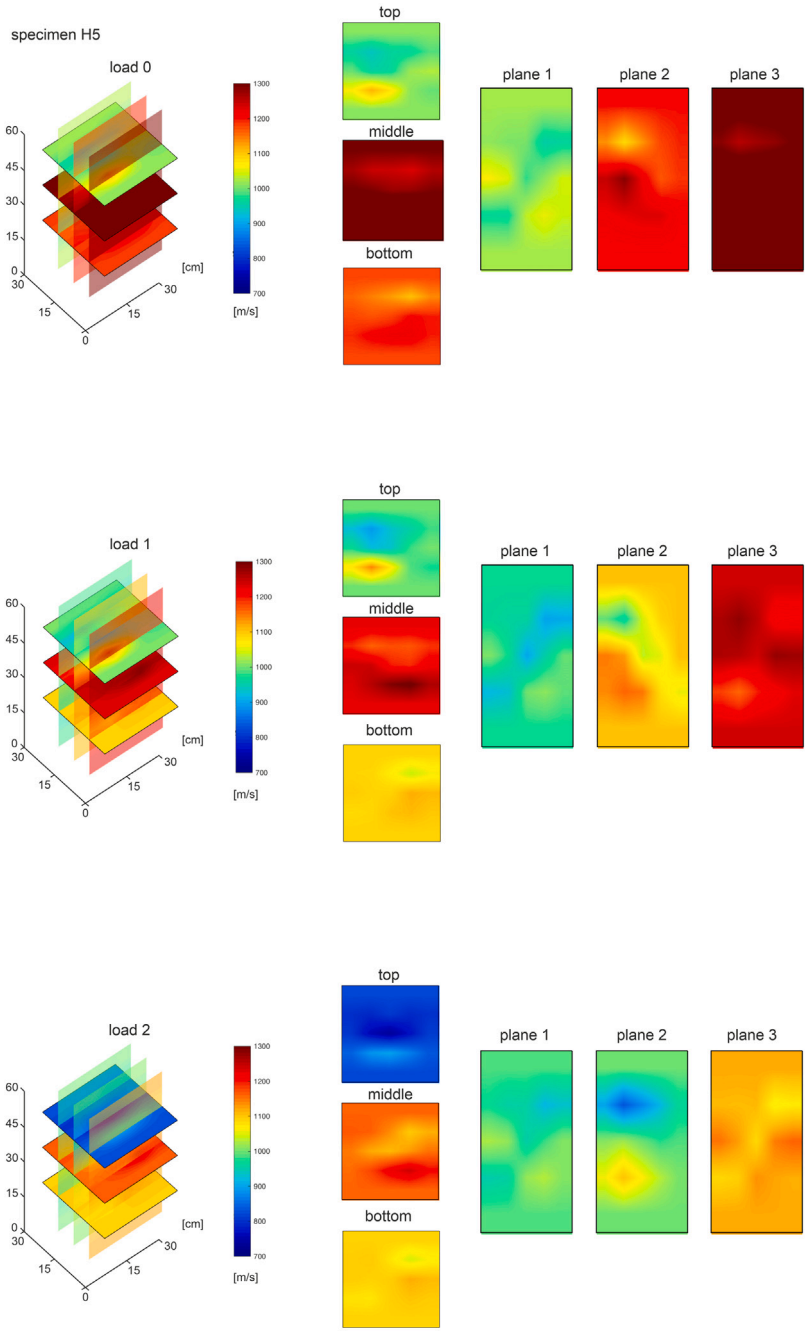


**Fig. 16.** Results from sonic tomography (specimen H5).

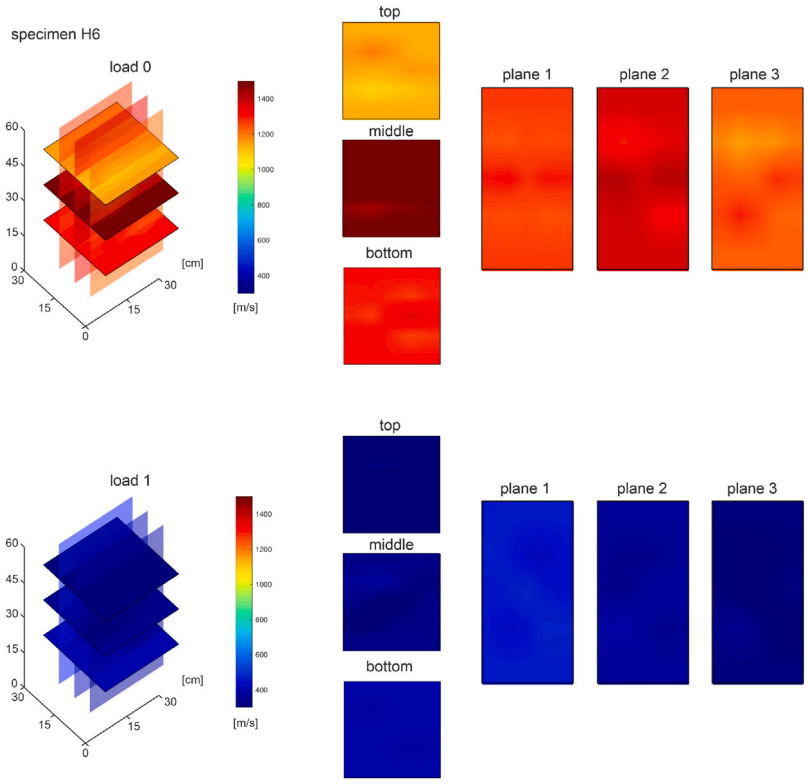


**Fig. 17.** Results from sonic tomography (specimen H6).

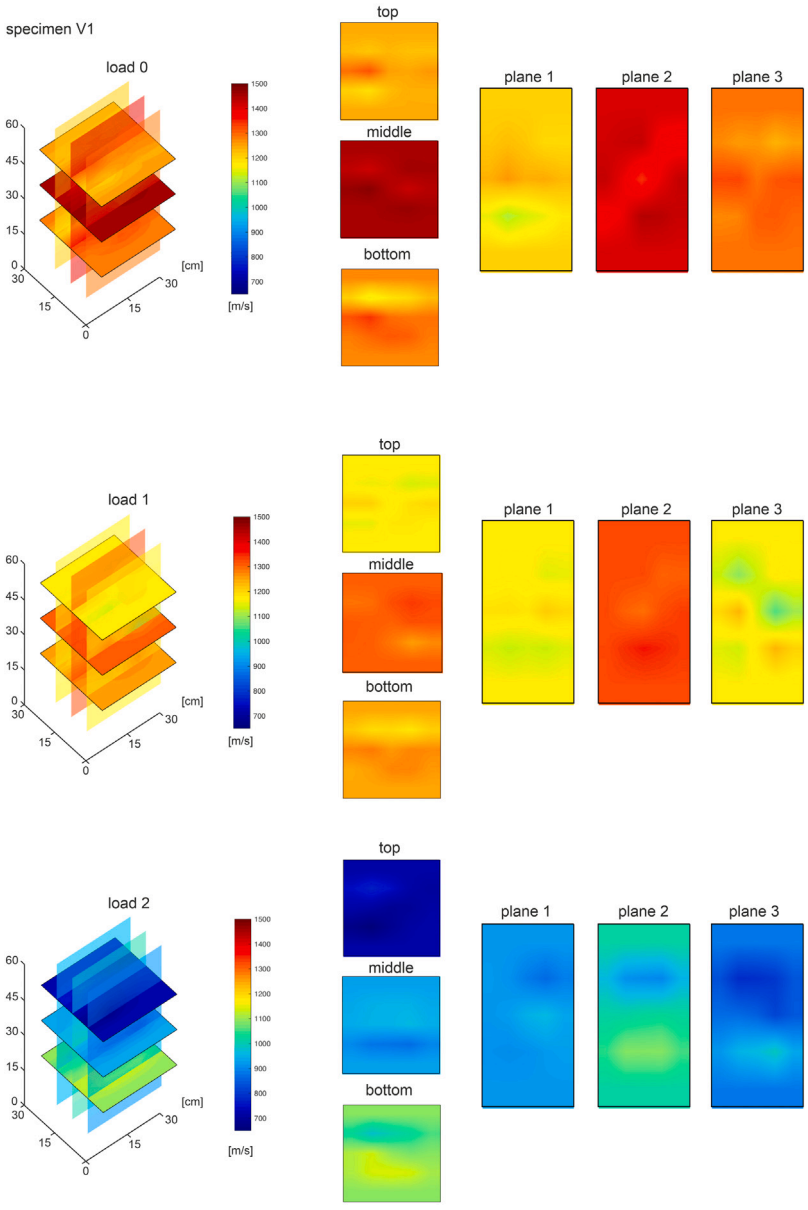


**Fig. 18.** Results from sonic tomography (specimen V1).

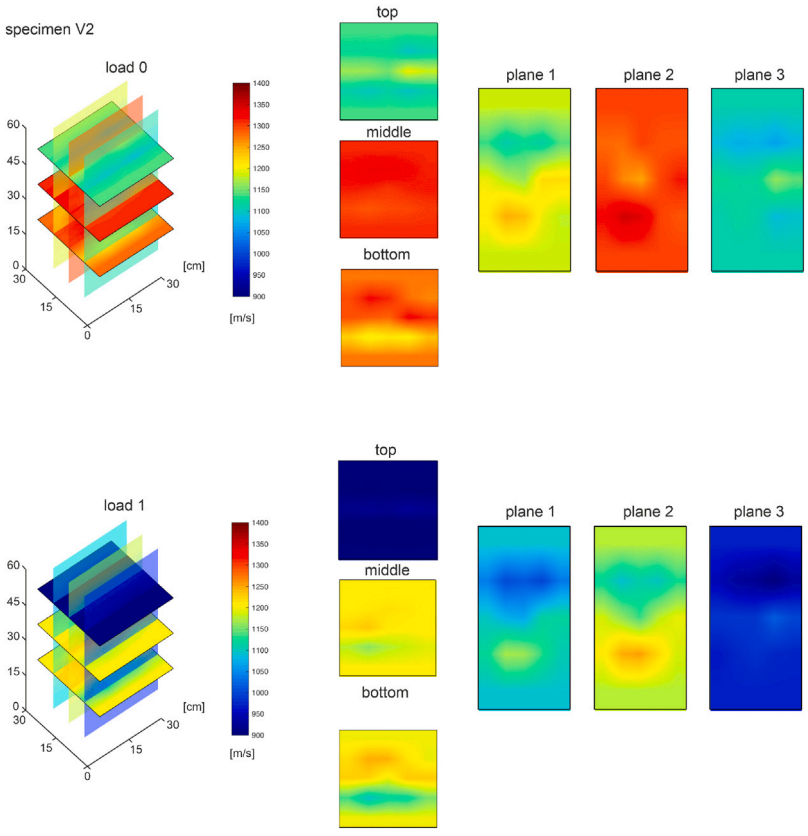


**Fig. 19.** Results from sonic tomography (specimen V2).

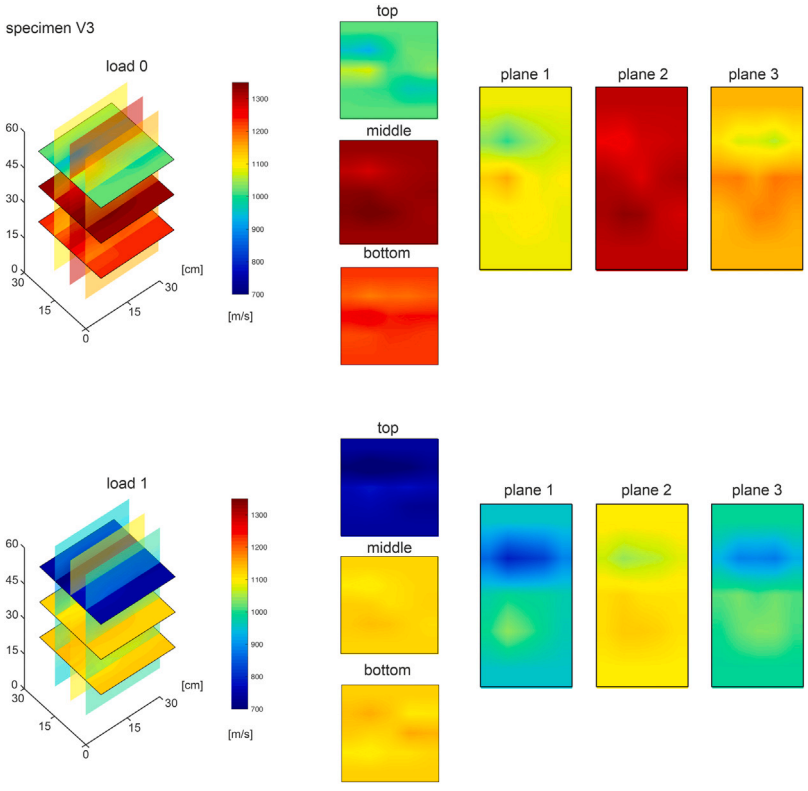


**Fig. 20.** Results from sonic tomography (specimen V3).

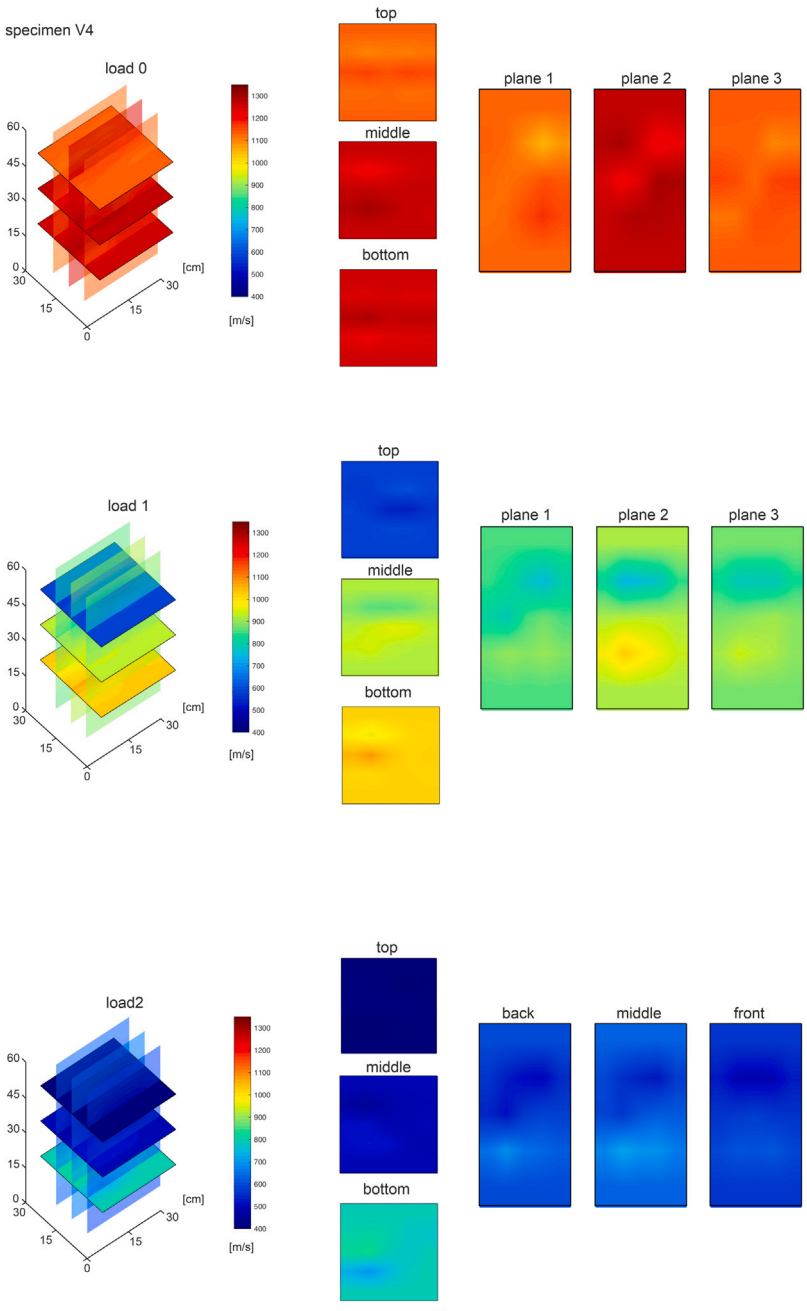


**Fig. 21.** Results from sonic tomography (specimen V4).

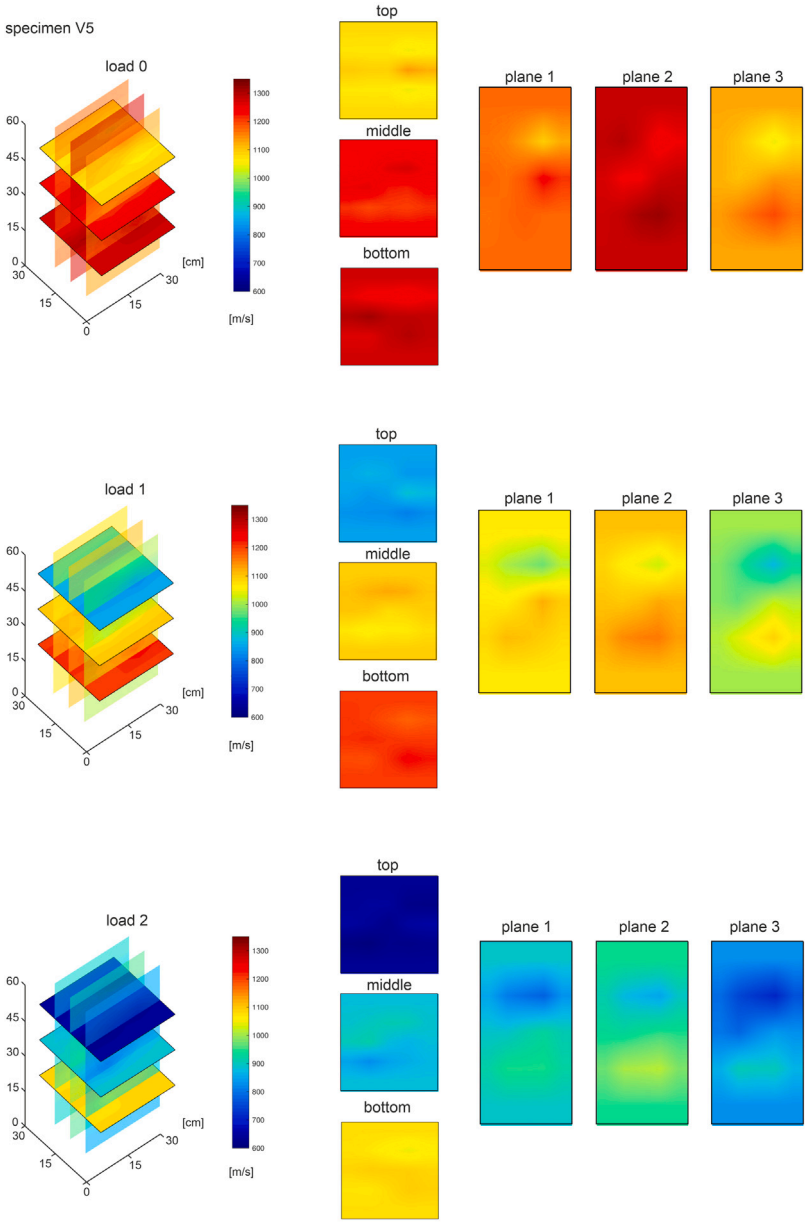


**Fig. 22.** Results from sonic tomography (specimen V5).

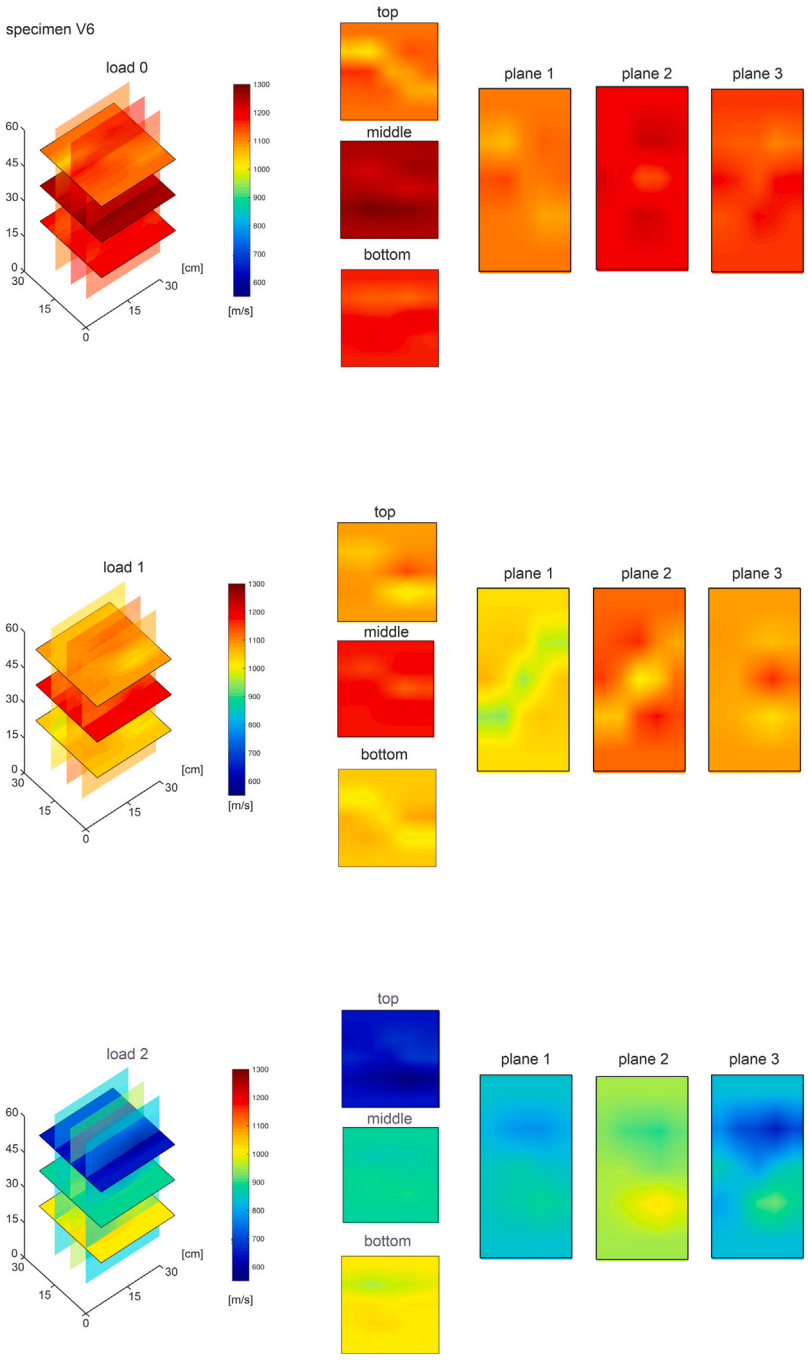


**Fig. 23.** Results from sonic tomography (specimen V6).

## References


[1] UNESCO. Earthen architecture in today's world proceedings of the UNESCO international colloquium on the conservation of world heritage earthen architecture. Paris: UNESCO Publishing; 2013, URL whc.unesco.org/document/126549.

[2] Jannat N, Hussien A, Abdullah B, Cotgrave A. Application of agro and non-agro waste materials for unfired earth blocks construction: A review. Constr Build Mater 2020;254:119346. http://dx.doi.org/10.1016/j.conbuildmat.2020.119346, URL https://www.sciencedirect.com/science/article/pii/S0950061820313519.

[3] Canivell J, Martin-del Rio JJ, Alejandre F, García-Heras J, Jimenez-Aguilar A. Considerations on the physical and mechanical properties of lime-stabilized rammed earth walls and their evaluation by ultrasonic pulse velocity testing. Constr Build Mater 2018;191:826–36. http://dx.doi.org/10.1016/J.CONBUILDMAT.2018.09.207, URL https://www.sciencedirect.com/science/article/pii/S0950061818323961#fn1.

[4] Martín-del Rio JJ, Canivell J, Falcón RM. The use of non-destructive testing to evaluate the compressive strength of a lime-stabilised rammed-earth wall: Rebound index and ultrasonic pulse velocity. Constr Build Mater 2020;242:118060. http://dx.doi.org/10.1016/J.CONBUILDMAT.2020.118060, URL https://www.sciencedirect.com/science/article/pii/S0950061820300659.

[5] Raavi SSD, Tripura DD. Ultrasonic pulse velocity and statistical analysis for predicting and evaluating the properties of rammed earth with natural and brick aggregates. Constr Build Mater 2021;298:123840. http://dx.doi.org/10.1016/j.conbuildmat.2021.123840, URL https://linkinghub.elsevier.com/retrieve/pii/S0950061821016007.

[6] Zhou T, Zhang H, Li B, Zhang L, Tan W. Evaluation of compressive strength of cement-stabilized rammed earth wall by ultrasonic-rebound combined method. J Build Eng 2023;68:106121. http://dx.doi.org/10.1016/J.JOBE.2023.106121.

[7] Bernat-Maso E, Teneva E, Escrig C, Gil L. Ultrasound transmission method to assess raw earthen materials. Constr Build Mater 2017;156:555–64. http://dx.doi.org/10.1016/J.CONBUILDMAT.2017.09.012, URL https://www.sciencedirect.com/science/article/pii/S095006181731803 2?via%3Dihub.

[8] Schuller M, Berra M, Atkinson R, Binda L. Acoustic tomography for evaluation of unreinforced masonry. Constr Build Mater 1997;11(3):199–204. http://dx.doi.org/10.1016/S0950-0618(97)00038-X.

[9] Binda L, Saisi A, Tiraboschi C. Application of sonic tests to the diagnosis of damaged and repaired structures. NDT E Int 2001;34(2):123–38. http://dx.doi.org/10.1016/S0963-8695(00)00037-2, URL https://www.sciencedirect.com/science/article/pii/S0963869500000372.

[10] Miranda LF, Rio J, Miranda Guedes J, Costa A. Sonic impact method – A new technique for characterization of stone masonry walls. Constr Build Mater 2012;36:27–35. http://dx.doi.org/10.1016/J.CONBUILDMAT.2012.04.018, URL https://www.sciencedirect.com/science/article/pii/S0950061812002206.

[11] Valluzzi MR, Cescatti E, Cardani G, Cantini L, Zanzi L, Colla C, Casarin F. Calibration of sonic pulse velocity tests for detection of variable conditions in masonry walls. Constr Build Mater 2018;192:272–86. http://dx.doi.org/10.1016/J.CONBUILDMAT.2018.10.073, URL https://www.sciencedirect.com/science/article/pii/S0950061818324346.

[12] Miranda L, Cantini L, Guedes J, Costa A. Assessment of mechanical properties of full-scale masonry panels through sonic methods. Comparison with mechanical destructive tests. Struct Control Health Monit 2016;23(2016):503–16. http://dx.doi.org/10.1002/stc.1783.

[13] Luchin G, Ramos LF, D'Amato M. Sonic tomography for masonry walls characterization. Int J Archit Herit 2020;14(4):589–604. http://dx.doi.org/10.1080/15583058.2018.1554723.

[14] Ortega J, Meersman MF, Aparicio S, Liébana JC, Martín R, Anaya JJ, González M. An automated sonic tomography system for the inspection of historical masonry walls. Open Res Eur 2023;3:1–29. http://dx.doi.org/10.12688/openreseurope.15769.1.

[15] Silva RA, Mendes N, Oliveira DV, Romanazzi A, Domínguez-Martínez O, Miranda T. Evaluating the seismic behaviour of rammed earth buildings from Portugal: From simple tools to advanced approaches. Eng Struct 2018;157:144–56. http://dx.doi.org/10.1016/J.ENGSTRUCT.2017.12.021, URL https://www.sciencedirect.com/science/article/pii/S0141029617321375?via%3Dihub#b0040.

[16] Rodríguez-Mariscal JD, Canivell J, Solís M. Evaluating the performance of sonic and ultrasonic tests for the inspection of rammed earth constructions. 2021;299. http://dx.doi.org/10.1016/j.conbuildmat.2021.123854.

[17] Zielińska M, Rucka M. Non-destructive assessment of masonry pillars using ultrasonic tomography. Materials 2018;11(12):2543. http://dx.doi.org/10.3390/MA11122543, 2018, Vol. 11, Page 2543. https://www.mdpi.com/1996-1944/11/12/2543/htmhttps://www.mdpi.com/1996-1944/11/12/2543.

[18] Zielińska M, Rucka M. Detection of debonding in reinforced concrete beams using ultrasonic transmission tomography and hybrid ray tracing technique. Constr Build Mater 2020;262:120104. http://dx.doi.org/10.1016/J.CONBUILDMAT.2020.120104.

[19] Couvreur L, Buzo A. Learn building impact Ø design and build with rammed earth. In: Erasmus+ project learnbiøn - learn building impact zero network (2015-2018). DEHESA TIERRA. Vol. 5, 2018.

[20] UNE-AENOR. UNE-EN ISO 17892-4. Geotechnical investigation and testing - laboratory testing of soil - Part 4: Determination of particle size distribution. Madrid, Spain: Asociación Española de Normalización y Certificación.

[21] CNS. UNE EN ISO 17892-12. Determinación del límite líquido y plástico de un suelo. Madrid, Spain: European Committee for Standardization; 2019.

[22] Oliveira EF, Melo SB, Dantas CC, Vasconcelos DA, Cadiz LF. Comparison among tomographic reconstruction with limited data. Int Nucl Atl Conf 2011;1–14, URL https://inis.iaea.org/search/search.aspx?orig_q=RN:43048827.

[23] Bui Q-B, Morel J-C. Assessing the anisotropy of rammed earth. Constr Build Mater 2009;23(9):3005–11. http://dx.doi.org/10.1016/j.conbuildmat.2009.04.011, URL http://www.sciencedirect.com/science/article/pii/S0950061809001445.

[24] Rodríguez-Mariscal JD, Canivell J, Solís M. Considerations on the use of ultrasonic pulse velocity, compressive and indirect tensile tests for the quality control of statically compressed earth samples. Int J Mason Res Innov 2022;7(5):460–81. http://dx.doi.org/10.1504/IJMRI.2022.125364.